2023 IEEE/ASME International Conference on
Advanced Intelligent Mechatronics (AIM)

Design and Validation of a Versatile High Torque Quasi-Direct Drive Hip Exoskeleton

Aakash Bajpai[1,2], Carlos Carrasquillo[1,2], Jessica Carlson[3], Julian Park[1], Divya Iyengar[1], Kinsey Herrin[1,2], Aaron J. Young[1,2], Anirban Mazumdar[1,2]

***Abstract*—The field of wearable robotics has made significant progress toward augmenting human functions from multi-modal ambulation to manual lifting tasks. However, most of these systems are designed to be task-specific and only focus on a single type of movement (e.g. ambulation). In this work, we design, fabricate, and characterize a versatile hip exoskeleton test-bed for lifting and ambulation tasks. The exoskeleton test-bed is actuated with custom-built quasi-direct drive actuators. We produce an orthotic interface to transmit high torques and assemble a custom mechatronic control system for the exoskeleton test-bed. We also detail controllers for level ground walking, incline walking, and symmetric knee to waist lifting. We quantify the actuator torque tracking performance quantified through benchtop and human experiments. During knee-to-waist cyclic lifting, the powered condition exhibited a 16.7% reduction in net metabolic cost compared to the no exoskeleton condition (3 subjects). For additional tasks (inclined walking, level-walking), the device provided metabolic reductions when compared with the unpowered case (single subject). These test-bed results illustrate the potential for versatile hip assistance and can be used to design future optimized devices.**

***Index Terms*—wearable robotics, exoskeleton, quasi-direct drive, metabolic cost, impedance control.**

I. Introduction

A. Overview

EXOSKELETONS are an area of growing interest and investment for improving locomotive economy, augmenting joint strength, and increasing endurance [1]. To achieve significant benefits, devices are often designed and controlled to address individual objectives [2]–[5]. Such specialized devices have had substantial success, ranging from significant reductions in EMG activation during lifting [6], [7] to improved economy during walking and running [8]. However, ambulation-specific assistive exoskeletons may not be powerful enough for movements such as lifting that require higher levels of assistance. Many occupations and settings require humans to perform a range of behaviors including locomotion over various terrain (flat ground, stairs, inclines), and diverse tasks (lifting, pushing, carrying). There is relatively little existing research on versatile exoskeleton systems that are designed to benefit people with regard to multiple movement types, such as both lifting and ambulation. Therefore, there is a need for a test-bed exoskeleton that would enable the study of versatile assistance across a broad range of tasks.

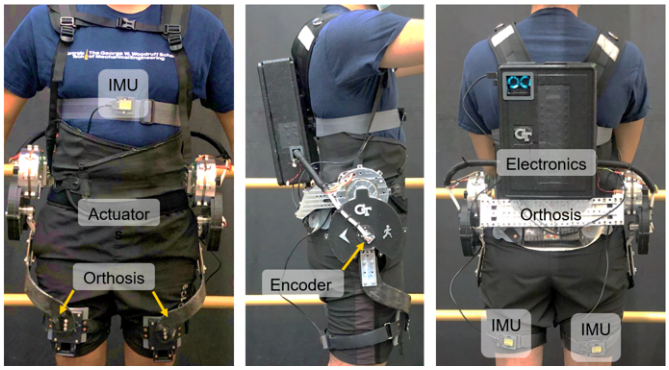

Figure 1: The Georgia Tech Agile Response Exoskeleton System (GT ARES) is a quasi-direct drive hip exoskeleton test-bed designed to achieve higher torques than most existing hip exoskeletons.

Versatile assistance requires different considerations than specialized assistance. Performing versatile tasks require a range of speeds and torques. Quasi-direct drive (QDD) actuators have recently shown promise [2], [9], [10] but existing wearable systems are generally still task limited in wearable robotics. In legged robot systems, QDD actuation has been shown to enable versatile performance [11]. QDDs have (1) the inherent benefit of transparency and (2) the capability for open-loop torque control. They are a promising actuation option for a versatile exoskeleton test-bed because their low gearing enables high speeds, high torques, and good force control bandwidth.

We have employed in-house fabricated quasi-direct drive actuators to develop an exoskeleton test-bed capable of versatile assistance at high levels of torque. In this paper, we describe the design of our actuator, orthosis, and mechatronics. We then outline quasi-stiffness-based impedance controllers. Next, we characterize the in-house designed and fabricated, high specific torque, quasi-direct drive actuators. This is done under static and dynamic conditions. Finally, we demonstrate the metabolic benefits of high exoskeleton assistance during high-speed walking, incline walking, and symmetric lifting.

B. Contributions

This research provides the following contributions. (1) We outline a quasi-direct drive hip exoskeleton test-bed that is the

This research is supported by the National Science Foundation (NSF) National Robotics Initiative (NRI) 1830498, US Department of Energy's Office of Environmental Management, NSF Traineeship Program 1545287, National Defense Science and Engineering Graduate (NDSEG) Fellowship, and Herbert P. Haley Fellowship. (Corresponding author: Aakash Bajpai - abajpai31@gatech.edu)

Authors are affiliated with the Georgia Institute of Technology Department of Mechanical Engineering[1] and Institute for Robotics and Intelligent Machines[2], as well as the University of Michigan Robotics Department[3].

Manuscript received January 2023; revised March 2023.

only design capable of providing up to 100% assistance for lifting and walking tasks. This system uses a unique spur-gear mechanical design that provides low-intrinsic impedance and low added mass. (2) We leverage biomechanical datasets to illustrate versatile impedance control and present new data-driven assistive impedance values for lifting and inclined walking augmentation. (3) We demonstrate, for the first time, a combination of absolute (vs. no exo) metabolic benefits during lifting combined with relative (vs. unpowered) metabolic benefits during inclined and level-walking. To summarize, this paper contributes a new physical system, and new data on assistance levels and control parameters for hip exoskeleton assistance across a range of tasks. While the lifting metabolic results with the specific device are exciting, this work also enables future designs tailored to the assistance levels identified in this work.

C. Previous Work: Biomechanical Considerations

1) Lifting: There is a wide range of applications for exoskeletons. With an emphasis from the US Defense Department, there has been a desire to augment human lifting capabilities [6], [7]. Assistance can be given at varying joints throughout the body [12] but has primarily been done through assisting lower limbs, commonly at the hip [13]. Hip exoskeletons also support the lower back [13], as lower back pain is a common workplace injury. Additionally, common lifting techniques include stooping, squatting, and variations in between the two [14]. During both variations of movement, the hip plays a significant role.

2) Ambulation: Significant research has been done to assist in an array of ambulation modes [1], [8]. Specifically, the hip and ankle joints are significant contributors of positive work output across speeds during walking and running [15]. Additionally, at increasingly higher inclines of walking, the hip is by far the largest contributor of positive work [16].

D. Previous Work: Design Considerations

There are several actuation methods that exoskeletons use to provide physical assistance [1], [8]. The actuation methods range from fully passive to fully active systems. Passive systems [17] do not add energy to the human's gait, instead they often passively absorb and distribute energy at different points in the gait cycle, different joints, etc. Fully active systems add energy through means of powered actuators. In our literature review, we have only found one exoskeleton to describe multi-functional benefits [18], however, this was a passive trunk exoskeleton that is inherently limited in control capability and therefore task variability.

Within powered actuation, many technologies have been implemented at the hip joint including hydraulics [19], pneumatics [20], and electro-mechanical systems [9], [21]. Electro-mechanical systems are the most common as they easily integrate with batteries and electronics [22]. Moreover, there are many transmission choices including cable-driven systems [4], [5], four-bar linkages [23], [24], belts [3], and planetary gears [9]. In some cases, compliant springs can provide benefits in the form of series elastic actuators (SEAs) [3], [5], [25].

Many wearable robotic systems are designed for cyclical ambulation modes which do not require high torques. These systems focus on reducing metabolic costs over long durations [8]. This has driven a desire for low-mass actuators which commonly employ small motors with large gear reductions. This approach has two key drawbacks: first, the peak speed of the system is reduced, and second, the reflected inertia can reduce force control bandwidth.

To balance metabolic energy expenditure with wide task application, we believe quasi-direct drive (QDD) systems offer great potential. QDD actuators are loosely defined as using a single-stage gear reduction of approximately 10:1 or less. QDD systems are capable of high bandwidth torque control. Moreover, due to QDDs low reflected inertia, they can be easily back-driven by the human operator when unpowered due to their high transparency. QDD actuators have show benefits in quadropeds [26], bipeds, [27], and on wearable systems [9], [10]. However, the versatility of QDD wearable systems remains unexplored.

II. QDD Hip Exoskeleton Test-bed Design

Drawing from previous biomechanics and exoskeleton design literature, we created a high torque, high specific torque, sagittal, QDD hip exoskeleton. The exoskeleton test-bed, shown in Fig. 1, has a total mass of 12.5 kg. The key contributors of mass are the actuators themselves (2.28 kg each), orthosis/interface components (5.94 kg), and electronics backpack (2 kg). While this test-bed has a relatively higher weight than existing hip exoskeletons, our literature review of hip exoskeletons show a range of system-level specific peak torques ranging from 5.7Nm/kg to 22.5Nm/kg [9], [21], [24], [25], [28]. Our device sits within this range at 11.2Nm/kg. In addition, our device provides the highest level of peak torque and a relatively high peak speed.

A. Actuator Design

The hip is known to achieve over 200 Nm in extension and nearly the same in flexion during maximum voluntary contractions (MVC) [30]. Thus, a design requirement of a peak torque of at least 50% of the hip's MVC (100 Nm) and a continuous torque of 20% of MVC (40Nm) was set when

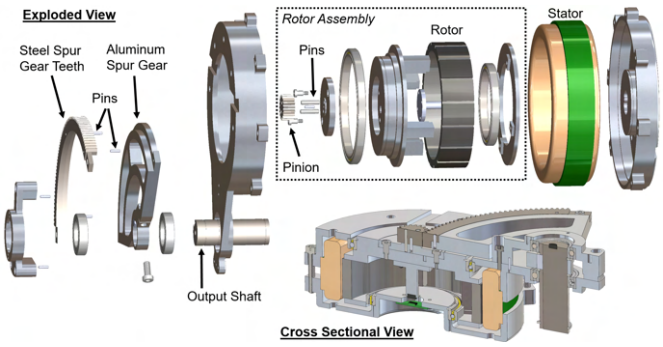

Figure 2: Renderings of the quasi-direct drive of ARES. The design features a high-torque brushless DC motor with custom housing and a partial spur-gear reduction.

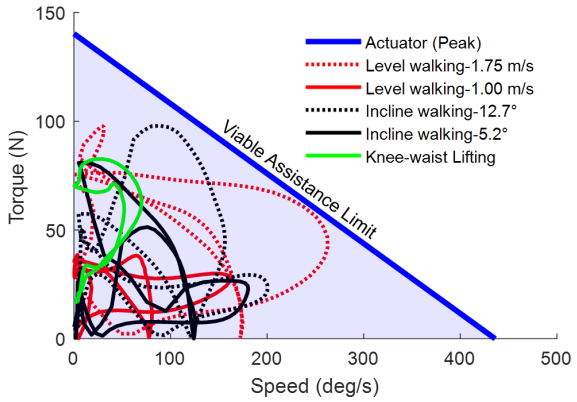

Figure 3: Varying speeds and torques must be achieved to ensure versatile benefits. Varying ambulation and lifting conditions are shown above for a 90kg participant. Ambulation data from N = 22 dataset [29] and lifting data from N = 12 dataset.

selecting the motor. The actuator was designed in-house, as off-the-shelf actuators did not have very high peak torques nor high specific torques (Nm/kg). The use of a frameless motor allowed for gearing and housing to be combined instead of increasing mass significantly by adding gearing to a self-contained motor. A frameless motor was selected, the Allied Motion MF0127 20mm stack stator and accompanying rotor. Peak torque and speed are particularly important to ensure the system is capable to assist a wide range of tasks. The selected gear reduction was 10:1, shown to achieve a variety of torques and speeds for various movements in Fig. 3. This figure illustrates the versatility of the system. Specifically, it shows how the device can potentially provide up to 100% assistance across a wide range of human behaviors (given a 90kg individual). This is a unique stand-alone (as opposed to tethered) test-bed capability that did not previously exist. The actuator mounting and housing components were then designed with a safety factor of 2 to withstand peak torque output. Renderings of the actuator design are provided in Fig. 2. The actuator weight is 2.28kg, with a rated torque of 42.1 Nm, and a peak torque of 140.27 Nm.

Actuator component fabrication was done in collaboration with the Georgia Tech Montgomery Machining Mall. The rotor is encapsulated by a rotor assembly that contains mating metals and bearings. As the rotor rotates, it moves an AR400 steel pinion gear, mated to an aluminum 7075 hub, through press-fit dowel pins. This aluminum hub is swappable for other gear ratios through shoulder bolts. This torque is then transferred to the output shaft via AR400 steel teeth, which are mated to AL 7075 through press-fit dowel pins. To further reduce weight a partial spur gear was designed with a bearing cap that went through the gear rather than around it. The design feature of combining steel teeth with an aluminum body for the gears allowed (1) significant weight savings and (2) an offset output shaft enabling the actuator mass to be closer to participants' COM. Moreover, this gear design weighs about half of a corresponding steel planetary gearing and is easier to manufacture with improved tolerance, as seen in Fig. 5.

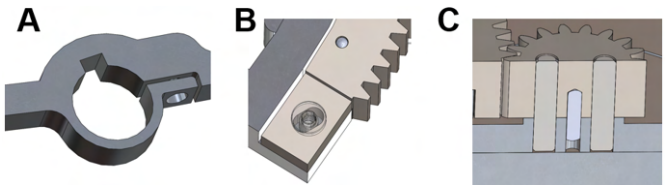

Figure 4: Key features of the ARES actuator. To ensure reduce the chance of play due to machining imprecision, a clamp (A) was designed into the partial spur gear and (B) spur steel gearing was on a slotted mechanism before pinning in place to enable effective teeth meshing. The input pinion gear was permanently fixed to a piece of 7075 aluminum (C) with two pins after a pilot pin was used to ensure the two parts were concentric.

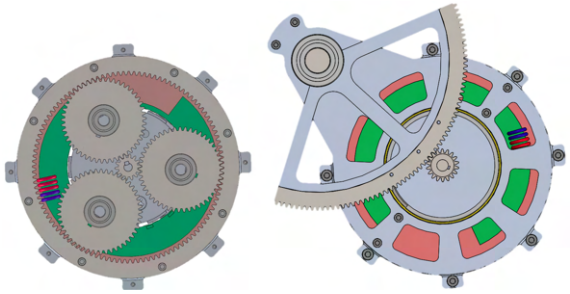

Figure 5: Early ARES actuator designs identified the weight could be reduced by utilizing a novel steel-aluminum mating (right) to reduce mass in comparison to conventional planetary gear systems (left).

$$\sigma_{yield} > \sigma_{tooth} = \frac{SF * F_{tooth}}{m * w_{face} * Y} \quad (1)$$

The gear thickness (from w_{face}) was driven by the Lewis bending equation [31] for stress on gear teeth (σ_{tooth}), where m is modulus, SF is safety factor, w_{face} is the face width, Y is the Lewis form factor (for pinion), and the force (F_{tooth}) was assumed to the peak of the motor. Dynamic effects known to happen at high speeds were neglected. Dowel pins at the steel-aluminum interface were sized to withstand shear force during peak torque. The output shaft size was determined as the minimum keyed shaft diameter to withstand the peak torsional stress applied by the actuator. The housing was designed with a keyed region on the bottom and top in addition to mounting holes so torque would be transferred through a geometric fit rather than bolts to the orthosis framing. A 3D printed gear case enclosed the gears for safety. Various geometric sizes were rounded to available stock parts on the market to enable reliable tolerances, for proper fitting. Custom shims were added to the rotor assembly to account for tolerance stack-up to minimize axial play while not over-constraining the system.

B. Orthosis Design

Orthosis design and fit are critical to exoskeleton performance. If an orthosis does not properly fit, it will limit the exoskeleton capabilities in terms of comfort, actuator bandwidth, and the length of experiments (due to discomfort). Additionally, varying body shapes should be accounted for in the design. The orthosis was designed in collaboration with

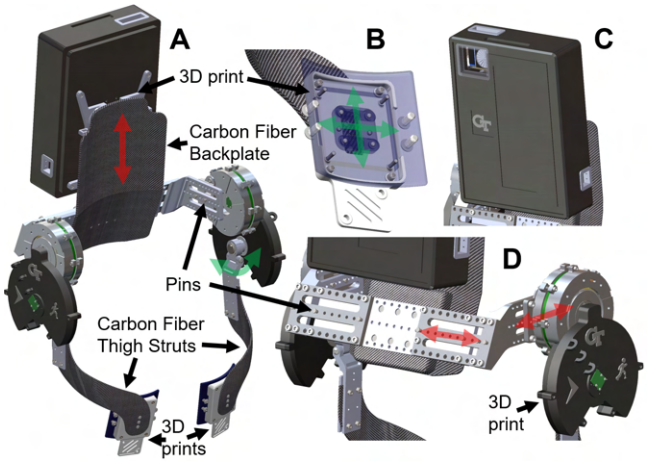

Figure 6: Images showing the custom carbon fiber-based orthosis. The system (A) is self-centering on the hip through a custom backplate that follows the lordotic curve between the lumbar spine and sacrum. This is conservative across most people and allows for most weight to be transferred close to the center of mass (COM). If the plate doesn't center well, backpack straps (if needed) can help adjust the vertical location of the actuators. Screws and pins allow for adaptation to varying subject sizes (D), as shown by the red arrows. Passive degrees of freedom at the thigh and hip (A, B), shown in green arrows, ensure comfortable, uninhibited joint function. The electronics are housed in a black foam container (C) with 3D printed inserts and adapters.

the GT Masters in Prosthetics and Orthotics (MSPO) program and other clinical staff to ensure safety and comfort.

Our custom orthosis uses custom carbon fiber components for the back plate, the pelvic struts, and the thigh arms that wrap from the actuator to the thighs, shown in Fig. 6. The back plate features an embedded 3D print to ensure a flat surface for the pelvic interface plate to attach to. Additionally, a non-stretch chest strap is included to prevent the back plate from separating from a participant's back and pushing outwards during flexion assistance. The thigh cuffs and lumbar spine orthosis allow for adjustability to various thigh circumferences with adjustable straps held in place by rivets. Actuator adjustment is possible through a clamped design where the pelvic carbon fiber struts are clamped to the actuator and to the interface plate. The thigh cuffs allow for passive movement to compensate for the misalignment of the moment arm with the hip joint. The electronics backpack is mounted to the backplate with an interfacing 3D printed part.

C. Mechatronics Design

All electronics are enclosed in a custom stiff styrofoam backpack. A vent is exposed with a 3D-printed insert for cooling airflow. Similar inserts are for cables and ports. The internal components are displayed in Fig. 7. The Allied Motion motors are controlled by Maxon EPOS 50/15 motor controllers. These perform proportional plus integral (PI) control on the current. A Raspberry Pi 4 8GB model commands current at 100 Hz through an analog signal (via I2C MCP4725 12-bit DACs). The Raspberry Pi collects from three Microstrain 3DM-GX5 AHRS IMUs and, if needed, four SPI AS5048A TS-EK-AB 14-bit encoders mounted on the input and output shafts of each actuator.

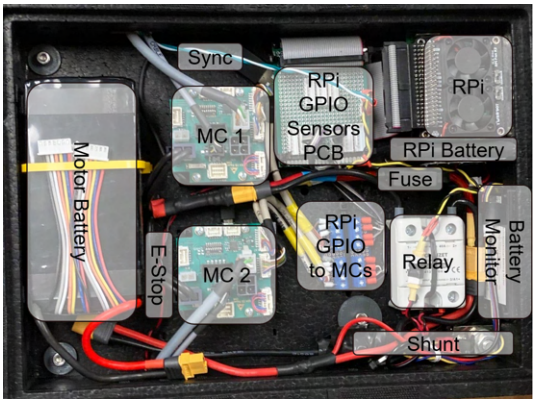

Figure 7: The electronics backpack is composed of two EPOS 50/15 motor controllers (MC), MaxAmps 3250mah 44.4V battery, Raspberry Pi (RPi) 4 and fan/battery hats, blade fuse, battery monitor, relay, and assorted breakouts and connectors for easy testing/debugging. Components are organized to keep mass close to the center of mass.

A Raspberry Pi 4 (kept cool with a fan hat) and sensors are powered by a Pi Sugar 2. Actuators are fed power through a blade fuse connected to a MaxAmps 3250 44.4V 12S battery. Power consumption, voltage levels, and amperage usage are viewed through a battery monitor on the backpack. A relay, controlled by an e-stop, can safely cut power from the motor controllers. The actuators receive power only if the Raspberry Pi is powered on and the e-stop is unlatched.

III. Exoskeleton Controls

Our exoskeleton test-bed uses a three-layer control architecture that is common in wearable robotics. The high-level controller is typically a mode classifier or an intention recognition algorithm. The mid-level controller maps the human subject and exoskeleton states to torque commands. The low-level controller regulates the current to the motors to provide effective torque tracking. In this paper, high-level intent is assumed to be known, so movement characteristics are prescribed to the mid-level controller. The three control layers are described below.

A. Low-Level Control: Closed Loop Current Control

The use of a single-stage gear reduction means that there is low friction in the QDD's transmission. Based on this property, output torque can be viewed as proportional to input current. This allows for open-loop torque control via closed-loop current control. Commercially available motor controllers can regulate current effectively and feature adjustable controller settings. The Maxon EPOS 50/15 has proportional and integral gains that were tuned during static testing to balance bandwidth with maximum magnitude. A key benefit of QDD actuators is that torque control can be performed using current feedback. The output torque can be assumed to be proportional to input current, reducing controller and sensing complexity.

B. Mid-Level Control: Quasi-stiffness Impedance Controller

Impedance controllers [32] are common in wearable robotic systems because they can provide safety, ease of implementation, and intuitive mapping of parameters to output response.

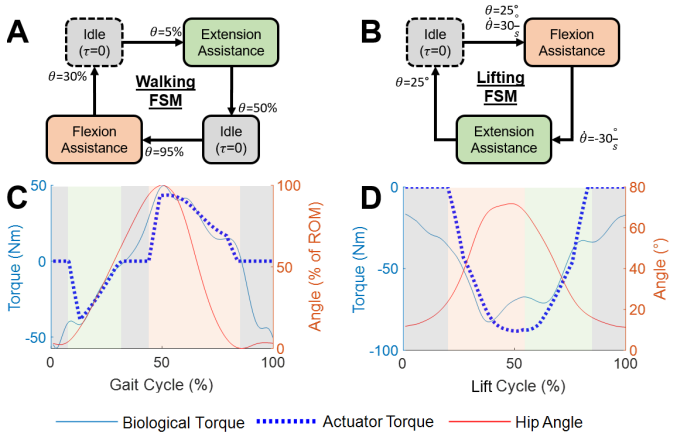

Figure 8: Example impedance controllers for (A/C) walking at average walking speed (1.25 $\frac{m}{s}$) and (B/D) symmetric knee-waist lifting with simulated biological data. Assistance profiles show 100% of biological assistance, displaying the impedance controllers' approximation of the biological torque. Finite state machine block diagrams (A/B) for walking and lifting for human experiments. Dotted idle blocks represent where the movement cycle begins. Switching criteria to enter the next state are noted near arrowheads. The shaded areas of the torque angle plots (C/D) correspond to the FSM blocks.

The human hip is known to act increasingly spring-like at higher walking speeds [29]. Interestingly, spring-like behaviors also exist for lifting tasks. Therefore quasi-stiffness-based impedance controllers offer the potential for versatile performance. The overall controller architecture can be kept fixed while the stiffness and equilibrium location can be modulated based on the human's behavior. While the controller may not be optimal for all tasks, it is a simple and effective controller that aligns well with the overall QDD framework.

To determine impedance parameters, we extracted hip joint angles and torques from an open-source ambulation dataset (N =22) [29] and an unpublished Georgia Tech lifting dataset (N = 12). Given a specific movement, different flexion and extension springs, k, and equilibrium angles, θ_0, were identified based on the angle-torque relationship. Next, the torque value (in $\frac{Nm}{kg}$ was multiplied by mass, m. The assistance contribution of the spring-based torque or damping-based torque was modulated through α and γ (set to 0), respectively.

$$\tau = m[\alpha * k(\theta - \theta_0) + \gamma * \beta(\dot{\theta})] \quad (2)$$

For both controllers, three states were defined including idle, extension, and flexion. The state machine for walking was tuned to maximize assistance during positive portions of movement. For lifting, the state machine was tuned during positive and negative portions of movement, as assistance during eccentric contractions is beneficial. Moving average filters for walking (5 point) and lifting (3 point) smoothed torque commands, shown in Fig. 8.

1) Impedance Controller Design for Walking: Ambulation controllers were created for level-ground (for varying speeds) and incline walking. To account for varying ranges of stride length during trials, angles were converted to a percentage of the range of motion (% ROM). This conversion was done with peak detection and a moving average filter. An automatic shutoff of torque was included when the ROM changed rapidly or stopped(such as from a trip, sudden movement, stop, etc). The switching criteria in the walking controller were defined to align with torque being applied during positive power portions of movement [15], a known method to reduce metabolic cost.

2) Impedance Controller Design for Lifting: During symmetric lifting, there was assistance during flexion (from knee to waist) and extension (from waist to knee). A cycle of knee-to-waist lifting with a 25lb weight was selected. During lifting, there are significant eccentric contractions, so assisting during negative power portions of movement is beneficial. Assistance engaged after movement initiation of lowering and raising.

Table I: Impedance Control Parameters for Various Tested Conditions

Movement	Phase	$k[\frac{N*m}{[\theta]*kg}]$	θ_{eq}
Level Walking 1.00$\frac{m}{s}$	Ext.	0.0071	63.65 %
	Fle.	0.0023	-58.68 %
Level Walking 1.25$\frac{m}{s}$	Ext.	0.0092	53.54 %
	Fle.	0.0033	-45.78 %
Level Walking 1.50$\frac{m}{s}$	Ext.	0.0118	51.66 %
	Fle.	0.0054	-21.53 %
Level Walking 1.75$\frac{m}{s}$	Ext.	0.0146	52.35 %
	Fle.	0.0082	-5.24 %
Ramp Walking 6.0°	Ext.	0.0149	51.91 %
	Fle.	0.0073	34.09 %
Knee-Waist Lifting	Ext.	0.0137	-5.75°
	Fle.	0.0125	-6.93°

k and θ_{eq} units are based on % of ROM (walking) or ° (lifting)

C. High-Level Controller

Our system's high-level control architecture modulates the impedance control parameters based on the human's behavior. This enables the system to provide versatile assistance across a range of tasks. For the scope of this work, the task was selected manually by the experimenter. In the future, this can be automated using intention recognition algorithms.

IV. Torque Tracking Validation

A. Benchtop Torque Tracking Testing

1) Static Testing: Benchtop framing was designed and fabricated to statically constrain the torque-controlled ARES actuator with a torque sensor (Futek TFF350 with IAA100 amplifier) to an optical table to determine the actuator frequency response. Torque signals were read by a National Instruments myRIO. A LabVIEW-based code recorded time-series readings and commands. The commanded torque trajectory, which mapped linearly to commanded current, was a pseudo-random input signal ranging from -20 to 20 Nm changing at a rate of 50Hz. After tuning PI gains and collecting data, a second-order model was fit to the experimental data. The motor controller tuning (P = 1000, I = 1250) resulted in a 20 Hz bandwidth, a damping ratio of 0.2032, and a peak magnitude of 8.0 dB.

2) Dynamic Testing: For dynamic testing (Fig. 9), instead of constraining the output shaft (with a torque sensor) of the motor to ground, it was attached to a position-controlled Harmonic Drive FHA-25C (with RTL servo driver). While the

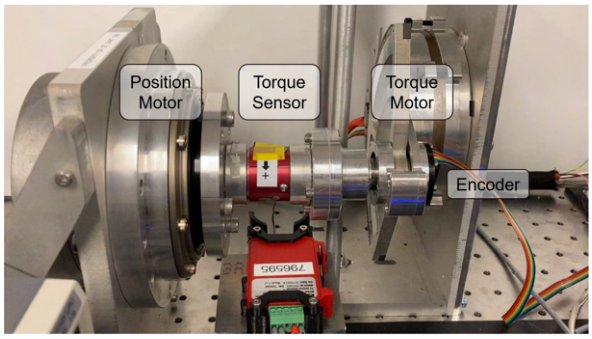

Figure 9: Dynamic bench-level setup to characterize the actuator.

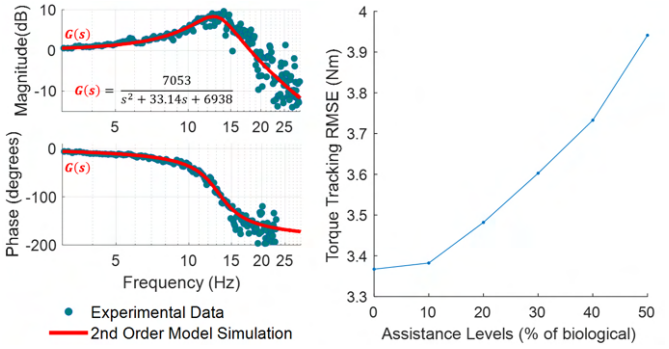

Figure 10: Bench-level bandwidth testing results for the actuator and transmission. Shown above are the static frequency response of the system fit with a second-order model (left) and dynamic torque tracking RMSE of walking at 1.25 $\frac{m}{s}$ at varying assistance levels.

actuator was powered by a Magna-Power 1.5kW single-phase power supply, the position-controlled motor was powered by 208 Vac 3-phase power. A Raspberry Pi 4 microcontroller commanded the impedance controller trajectory (angle from output shaft encoder) and a myRIO recorded torque responses. The impedance controllers' spring constants were designed to assist 1.25 $\frac{m}{s}$ walking at varying assistance levels (Fig. 10).

B. Human Validation: Torque Tracking

RMSE error of torque tracking is dependent on the trajectory of the reference torque signal. Thus, simplifying torque tracking to a single number describing the torque error is incomplete. We, therefore, tested the system at a range of assistance levels and walking speeds on a single male participant who provided informed consent under a Georgia Tech approved IRB protocol (H18272). Conditions included 0% (zero impedance mode), 10, 20, 30, 40, and 50% of biological extension torque ($\frac{1}{2}$ multiplier for flexion) on speeds including 1.00, 1.25, 1.5, 1.75$\frac{m}{s}$. One minute of steady-state walking was recorded for each condition. As assistance and walking speed increase, torque tracking error increases (Fig. 11).

V. Human Validation: Ambulation and Lifting

The final set of experiments in this work focused on evaluating the overall performance on human subjects. To explore versatile performance, we focused on three core behaviors: 1) knee-to-waist lifting, 2) inclined walking, and 3) level-ground high-speed walking. These behaviors were chosen

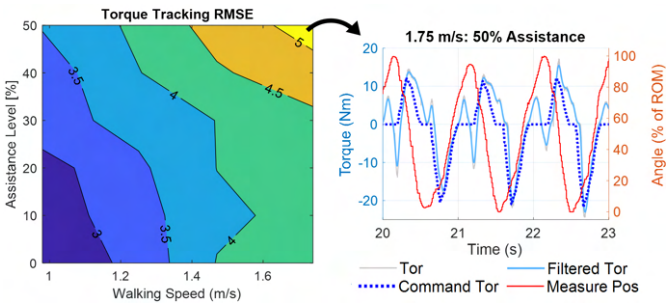

Figure 11: Torque tracking RMSE results for walking at various speeds and assistance levels (left). The highest speed and assistance combination is also displayed (right).

because they are substantially different from each other and are behaviors where the hip joint produces significant mechanical work. It was hypothesized that the hip exoskeleton testbed would provide metabolic benefits for these tasks. Our quantitative metric of performance was metabolic cost. While EMG is a common output metric used to measure the efficacy of wearable robots, reductions in EMG activation of a subset of muscles do not account for load redistribution effects between joints. Alternatively, metabolic cost is a holistic measurement as it is related to the body's total energy expenditure and can account for work transfer between joints. This is considered the gold standard for ambulation but requires a steady state movement to collect. We found that cyclic lifting was found to converge to a steady state after approximately two minutes. Metabolic cost was selected as the outcome metric and was estimated through indirect calorimetry with a COSMED K5 unit. Reported values are calculated (Brockway equation [33]) from the last two minutes of six-minute trials.

Four male participants (76-91kg) provided informed consent to participate in the study under a Georgia Tech approved IRB protocol (IRB H21228). One participant (AB00) was tested to determine the ratio of extension and flexion assistance beneficial for metabolic cost reductions, shown in Fig. 13 A-F. Three different participants (AB01-03) were tested for lifting,

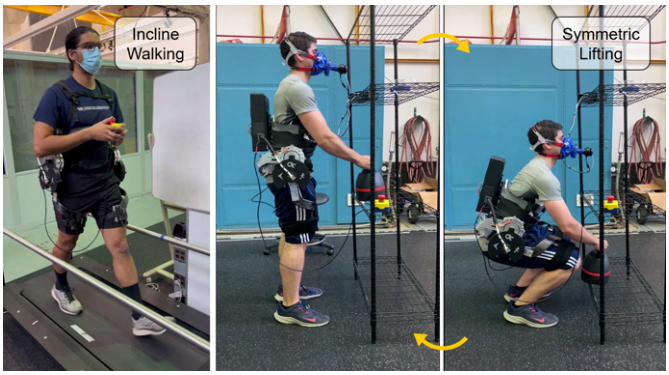

Figure 12: Incline walking (left) was conducted at the maximum incline of a Tufftread treadmill (6.0°). The periodic motion completed during lifting is shown (center and right). Participants started with the 25 lb kettlebell weight at waist level. Then every 10 seconds, a tone would prompt the participant to lift the weight with both hands off a shelf, lower the weight, tap on a shelf below, then raise the weight back to the top shelf, let go, and wait for the next tone.

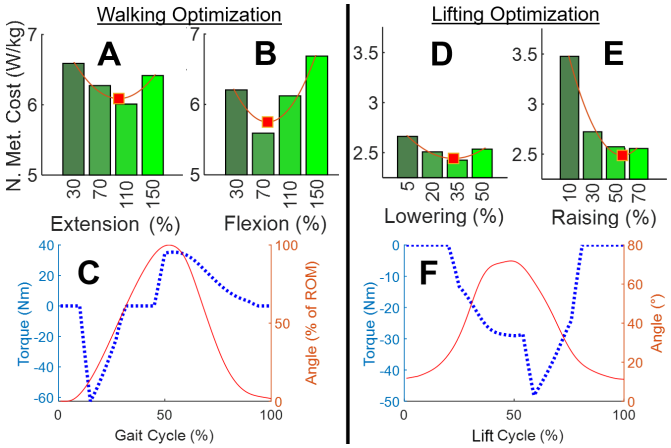

Figure 13: Quadratic fits (red lines) determine the net metabolic cost minima (red squares). Walking extension (A) and flexion (B) were optimized at 1.75 $\frac{m}{s}$ and the resulting tuning was used for AB00's incline walking (C). The lifting lowering (D) and raising (E) metabolic cost minima tuned AB00's lifting assistance profile (F).

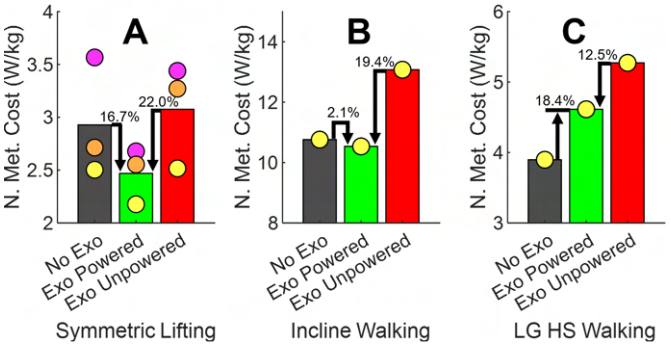

Figure 14: The net metabolic cost is reported for (A) symmetric cyclic knee-waist lifting, (B) incline walking at 6 degrees at 1$\frac{m}{s}$, and (C) high-speed walking at 1.75$\frac{m}{s}$. Average and individual (points) net metabolic costs are displayed for each condition.

one of whom (AB02) was also tested on incline walking and level-ground high-speed walking. Tuning and collection trials were randomized and repeated (ABCCBA design) to mitigate fatigue effects. Standing trials were taken at the beginning and end of experiments to calculate the net metabolic cost. The three collection conditions included a no exoskeleton, exoskeleton powered, and exoskeleton unpowered, as seen in Fig. 14. Participants were acclimated to the device for all collection conditions for at least 15 minutes per condition.

A. Assistance Magnitude Tuning

For cyclic lifting, there is no existing literature indicating the best profile to reduce metabolic cost. Therefore, we conducted an N=1 study to determine a preferred ratio of assistance waist to knee (flexion) and knee to waist (extension) assistance. A range of assistance levels was selected from low to high assistance, shown in Fig. 13. These assistance sweeps are enabled by the broad capability of the testbed device. Smaller devices would not produce large levels of assistance. The optimum ratio of flexion to extension assistance (32.8:55.8) was found. Finally, overall magnitude multipliers were tuned per novel participant for comfort (AB01/02: 1, AB03: 1.2).

During walking at a set speed on the treadmill, people prefer to minimize an objective function, approximated by metabolic cost [34]. We recorded AB00 preference (70% flexion and 110 % extension) and this matched well with the optimum ratio (76.7:98.7). Therefore, preference was used to tune assistance magnitude during subsequent walking tests. AB02 preferred magnitudes of 1.1 in flexion and 0.9 in extension.

B. Versatile Benefits

Given that everyday human movement aims to satisfy varying objectives, assistive wearable systems must be capable of providing benefits over many tasks. The results show that the GT ARES is beneficial during lifting compared to not wearing the device, as a 16.7% metabolic reduction was observed. This could motivate exoskeletons of similar design to be used in automotive, construction, and other industries which require manual materials handling and ambulation. In these operational environments, given that personnel may wear an analogous device, it is important to examine how to reduce the metabolic costs of other behaviors. In this work, we examined inclined walking and level-ground high-speed walking for a single subject. The results show how the exoskeleton controller can be used to reduce the metabolic cost of performing the new activity while wearing the device. For both incline walking and level-ground high-speed walking, the use of impedance-controlled assistance reduced metabolic effort when compared to exo unpowered. Specifically, the device provided a 19.4% reduction versus unpowered during inclined walking. Promisingly, the single-subject result also showed a 2.1 % reduction in metabolic cost over the no-exo condition. This is an area for further exploration. Lastly, the device provided a 12.5% reduction versus unpowered during level-ground high-speed walking. There was an increased metabolic cost associated with the device during level walking (18.4%). This is likely due to the fact that there are no intrinsic work requirements for level-ground walking [35]. This implies that the specific device architecture is not well-aligned with systems that only focus on level-ground walking.

VI. Future Work

To further reduce metabolic cost in the powered exoskeleton condition could utilize human-in-the-loop optimization on metabolic cost to adjust control parameters. Significant performance benefits from optimization have been seen in incline walking [35] and may present during lifting tasks. Moreover, the benefits of the GT ARES are more prominent during lifting as the weight of the exoskeleton has relatively less impact on metabolic cost. Reducing the weight of the orthosis, framing, and electronic components could lead to substantial metabolic benefits. Finally, there is a tradeoff between exoskeleton actuator bandwidth and orthosis comfort. A stiffer orthosis interface, while more uncomfortable, would allow for better torque tracking (such as at high-speed walking seen in Fig. 11) and likely better metabolic outcomes.

VII. Conclusion

As wearable robotic technologies are adopted in broader society it is important to consider how they perform in multiple

contexts. The QDD hip exoskeleton test-bed presented in this paper was designed to be a testbed system to augment various human movements at high levels of assistance. This device was combined with new data-driven task-specific impedance controllers. The overall system provided two core results. First, the device demonstrated metabolic benefits for lifting (versus no-exo). Second, the device showed metabolic improvements (versus un-powered) for inclined walking and level-walking. This shows that given a need for lifting assistance, hip assistance can still provide relative benefit for other tasks. In addition, the device was used to identify effective assistance levels. These assistance levels can be used to design optimized systems that could provide further metabolic improvements.

REFERENCES

[1] H. Herr, "Exoskeletons and orthoses: classification, design challenges and future directions," *Journal of NeuroEngineering and Rehabilitation*, vol. 6, no. 1, Jun 2009.

[2] S. Chen, D. T. Stevenson, S. Yu, M. Mioskowska, J. Yi, H. Su, and M. Trkov, "Wearable Knee Assistive Devices for Kneeling Tasks in Construction," *IEEE/ASME Transactions on Mechatronics*, vol. 26, no. 4, pp. 1989–1996, 2021.

[3] L. Liu, Z. Hong, B. Penzlin, B. J. E. Misgeld, C. Ngo, L. Bergmann, and S. Leonhardt, "Low Impedance-Guaranteed Gain-Scheduled GESO for Torque-Controlled VSA With Application of Exoskeleton-Assisted Sit-to-Stand," *IEEE/ASME Transactions on Mechatronics*, vol. 26, no. 4, pp. 2080–2091, 2021.

[4] H. Li, D. Sui, H. Ju, Y. An, J. Zhao, and Y. Zhu, "Mechanical Compliance and Dynamic Load Isolation Design of Lower Limb Exoskeleton for Locomotion Assistance," *IEEE/ASME Transactions on Mechatronics*, vol. 27, no. 6, pp. 5392–5402, 2022.

[5] T. Zhang, K. Feng, B. Zeng, and Z. Gong, "Design and Validation of a Lightweight Soft Hip Exosuit With Series-Wedge-Structures for Assistive Walking and Running," *IEEE/ASME Transactions on Mechatronics*, vol. 27, no. 5, pp. 2863–2874, 2022.

[6] H. Kazerooni, "A review of the Exoskeleton and human augmentation technology," *ASME 2008 Dynamic Systems and Control Conference, Parts A and B*, 2008.

[7] W. Wei, S. Zha, Y. Xia, J. Gu, and X. Lin, "A Hip Active Assisted Exoskeleton That Assists the Semi-Squat Lifting," *Applied Sciences*, vol. 10, no. 7, 2020. [Online]. Available: https://www.mdpi.com/2076-3417/10/7/2424

[8] G. S. Sawicki, O. N. Beck, I. Kang, and A. J. Young, "The exoskeleton expansion: improving walking and running economy," *Journal of NeuroEngineering and Rehabilitation*, vol. 17, no. 1, Feb 2020.

[9] S. Yu, T.-H. Huang, X. Yang, C. Jiao, J. Yang, Y. Chen, J. Yi, and H. Su, "Quasi-Direct Drive Actuation for a Lightweight Hip Exoskeleton With High Backdrivability and High Bandwidth," *IEEE/ASME Transactions on Mechatronics*, vol. 25, no. 4, pp. 1794–1802, 2020.

[10] H. Zhu, C. Nesler, N. Divekar, V. Peddinti, and R. D. Gregg, "Design Principles for Compact, Backdrivable Actuation in Partial-Assist Powered Knee Orthoses," *IEEE/ASME Transactions on Mechatronics*, vol. 26, no. 6, p. 3104–3115, Oct 2021.

[11] C. G. Hobart, A. Mazumdar, S. J. Spencer, M. Quigley, J. P. Smith, S. Bertrand, J. Pratt, M. Kuehl, and S. P. Buerger, "Achieving Versatile Energy Efficiency With the WANDERER Biped Robot," *IEEE Transactions on Robotics*, vol. 36, no. 3, pp. 959–966, 2020.

[12] A. Ali, V. Fontanari, W. Schmoelz, and S. K. Agrawal, "Systematic review of back-support exoskeletons and soft robotic suits," *Frontiers in Bioengineering and Biotechnology*, vol. 9, 2021.

[13] J. K. Proud, D. T. H. Lai, K. L. Mudie, G. L. Carstairs, D. C. Billing, A. Garofolini, and R. K. Begg, "Exoskeleton Application to Military Manual Handling Tasks," *Human Factors*, vol. 64, no. 3, 2022.

[14] R. Burgess-Limerick, "Squat, stoop, or something in between?" *International Journal of Industrial Ergonomics*, vol. 31, no. 3, 2003.

[15] D. J. Farris and G. S. Sawicki, "The mechanics and energetics of human walking and running: A joint level perspective," *Journal of The Royal Society Interface*, vol. 9, no. 66, p. 110–118, 2011.

[16] R. W. Nuckols, K. Z. Takahashi, D. J. Farris, S. Mizrachi, R. Riemer, and G. S. Sawicki, "Mechanics of walking and running up and downhill: A joint-level perspective to guide design of lower-limb exoskeletons," *PLOS ONE*, vol. 15, no. 8, pp. 1–20, 08 2020.

[17] B. Zhang, T. Liu, B. Zhang, and M. G. Pecht, "Recent Development of Unpowered Exoskeletons for Lower Extremity: A Survey," *IEEE Access*, vol. 9, pp. 138 042–138 056, 2021.

[18] S. J. Baltrusch, J. H. van Dieën, S. M. Bruijn, A. S. Koopman, C. A. van Bennekom, and H. Houdijk, "The effect of a passive trunk exoskeleton on metabolic costs during lifting and walking," *Ergonomics*, vol. 62, no. 7, p. 903–916, 2019.

[19] A. Zoss, H. Kazerooni, and A. Chu, "On the mechanical design of the Berkeley Lower Extremity Exoskeleton (BLEEX)," in *2005 IEEE/RSJ International Conference on Intelligent Robots and Systems*, 2005.

[20] C. L. Lewis and D. P. Ferris, "Invariant hip moment pattern while walking with a robotic hip exoskeleton," *Journal of Biomechanics*, vol. 44, no. 5, p. 789–793, Mar 2011.

[21] T. Zhang, M. Tran, and H. Huang, "Design and Experimental Verification of Hip Exoskeleton With Balance Capacities for Walking Assistance," *IEEE/ASME Transactions on Mechatronics*, vol. 23, no. 1, pp. 274–285, 2018.

[22] T.-H. Huang, S. Zhang, S. Yu, M. K. MacLean, J. Zhu, A. Di Lallo, C. Jiao, T. C. Bulea, M. Zheng, and H. Su, "Modeling and Stiffness-Based Continuous Torque Control of Lightweight Quasi-Direct-Drive Knee Exoskeletons for Versatile Walking Assistance," *IEEE Transactions on Robotics*, vol. 38, no. 3, pp. 1442–1459, 2022.

[23] T. Kim, M. Jeong, and K. Kong, "Bioinspired Knee Joint of a Lower-Limb Exoskeleton for Misalignment Reduction," *IEEE/ASME Transactions on Mechatronics*, vol. 27, no. 3, pp. 1223–1232, 2022.

[24] M. K. Ishmael, D. Archangeli, and T. Lenzi, "A Powered Hip Exoskeleton With High Torque Density for Walking, Running, and Stair Ascent," *IEEE/ASME Transactions on Mechatronics*, vol. 27, no. 6, pp. 4561–4572, 2022.

[25] I. Kang, R. R. Peterson, K. R. Herrin, A. Mazumdar, and A. J. Young, "Design and Validation of a Torque-Controllable Series Elastic Actuator-Based Hip Exoskeleton for Dynamic Locomotion," *Journal of Mechanisms and Robotics*, vol. 15, no. 2, 06 2022.

[26] S. Seok, A. Wang, M. Y. Chuah, D. J. Hyun, J. Lee, D. M. Otten, J. H. Lang, and S. Kim, "Design Principles for Energy-Efficient Legged Locomotion and Implementation on the MIT Cheetah Robot," *IEEE/ASME Transactions on Mechatronics*, vol. 20, no. 3, pp. 1117–1129, 2015.

[27] A. Mazumdar, S. J. Spencer, C. Hobart, J. Dabling, T. Blada, K. Dullea, M. Kuehl, and S. P. Buerger, "Synthetic Fiber Capstan Drives for Highly Efficient, Torque Controlled, Robotic Applications," *IEEE Robotics and Automation Letters*, vol. 2, no. 2, pp. 554–561, 2017.

[28] K. Seo, J. Lee, Y. Lee, T. Ha, and Y. Shim, "Fully autonomous hip exoskeleton saves metabolic cost of walking," *2016 IEEE International Conference on Robotics and Automation (ICRA)*, 2016.

[29] J. Camargo, A. Ramanathan, W. Flanagan, and A. Young, "A comprehensive, open-source dataset of lower limb biomechanics in multiple conditions of stairs, ramps, and level-ground ambulation and Transitions," *Journal of Biomechanics*, vol. 119, p. 110320, Apr 2021.

[30] D. E. Anderson, M. L. Madigan, and M. A. Nussbaum, "Maximum voluntary joint torque as a function of joint angle and angular velocity: Model development and application to the lower limb," *Journal of Biomechanics*, vol. 40, no. 14, p. 3105–3113, May 2007.

[31] R. G. Budynas, J. K. Nisbett, and J. E. Shigley, *Shigley's Mechanical Engineering Design*. McGraw-Hill, 2011.

[32] N. Hogan, "Impedance Control: An approach to manipulation," *1984 American Control Conference*, 1984.

[33] B. Jm, "Derivation of formulae used to calculate energy expenditure in man," vol. 41, no. 6, pp. 463–471, 1987.

[34] J. E. Bertram and A. Ruina, "Multiple walking speed–frequency relations are predicted by constrained optimization," *Journal of Theoretical Biology*, vol. 209, no. 4, p. 445–453, 2001.

[35] P. W. Franks, G. M. Bryan, R. Reyes, M. P. O'Donovan, K. N. Gregorczyk, and S. H. Collins, "The Effects of Incline Level on Optimized Lower-Limb Exoskeleton Assistance: A Case Series," *IEEE Transactions on Neural Systems and Rehabilitation Engineering*, vol. 30, pp. 2494–2505, 2022.